

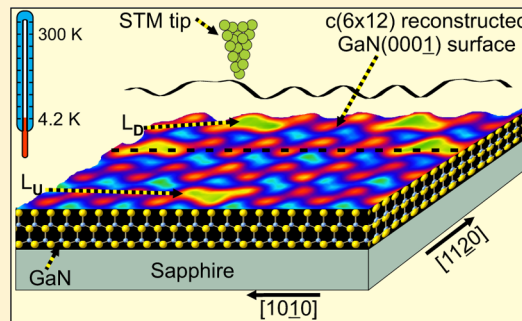
Native Gallium Adatoms Discovered on Atomically-Smooth Gallium Nitride Surfaces at Low Temperature

Khan Alam, Andrew Foley, and Arthur R. Smith*

Nanoscale and Quantum Phenomena Institute, Department of Physics and Astronomy, Ohio University, Athens, Ohio 45701, United States

S Supporting Information

ABSTRACT: In advanced compound semiconductor devices, such as in quantum dot and quantum well systems, detailed atomic configurations at the growth surfaces are vital in determining the structural and electronic properties. Therefore, it is important to investigate the surface reconstructions in order to make further technological advancements. Usually, conventional semiconductor surfaces (e.g., arsenides, phosphides, and antimonides) are highly reactive due to the existence of a high density of group V (anion) surface dangling bonds. However, in the case of nitrides, group III rich growth conditions in molecular beam epitaxy are usually preferred leading to group III (Ga)-rich surfaces. Here, we use low-temperature scanning tunneling microscopy to reveal a uniform distribution of native gallium adatoms with a density of 0.3%–0.5% of a monolayer on the clean, as-grown surface of nitrogen polar GaN(000 $\bar{1}$) having the centered 6 × 12 reconstruction. Unseen at room temperature, these Ga adatoms are strongly bound to the surface but move with an extremely low surface diffusion barrier and a high density saturation coverage in thermodynamic equilibrium with Ga droplets. Furthermore, the Ga adatoms reveal an intrinsic surface chirality and an asymmetric site occupation. These observations can have important impacts in the understanding of gallium nitride surfaces.



In addition, the authors mention that these Ga adatoms are strongly bound to the surface but move with an extremely low surface diffusion barrier and a high density saturation coverage in thermodynamic equilibrium with Ga droplets. Furthermore, the Ga adatoms reveal an intrinsic surface chirality and an asymmetric site occupation. These observations can have important impacts in the understanding of gallium nitride surfaces.

KEYWORDS: gallium nitride surface, native adatoms, surface diffusion, chirality, low temperature scanning tunneling microscopy, molecular beam epitaxy

The ground-breaking development of gallium nitride by Nakamura and co-workers has led to major advances in lighting technology and was recently rewarded with the Nobel Prize in physics.^{1–3} Gallium nitride has a wide range of current applications, including for ultraviolet and blue light-emitting diodes, white lighting, lasers, power transistors and integrated circuit technologies.^{1,4,5} In addition, GaN has potential applications in the areas of chemical and biological sensors based on its biocompatibility, semiconducting nature, and physical and chemical stability.^{6–8} The key to applications in these latter cases is an improved understanding of the GaN surface and its properties including stoichiometry, electronic states, surface diffusion, and even chirality.^{9–12}

The GaN surface is of course the key to GaN thin film growth, and among various growth models that have been proposed, surface diffusive growth was investigated by Zywietz et al.^{13,14} Surface diffusion and diffusion barriers calculated and compared for Ga-terminated versus N-terminated surfaces are particularly helpful in understanding the experimental fact that GaN growth by molecular beam epitaxy (MBE) performed under Ga-rich conditions leads to the best quality and atomically smoothest GaN surfaces and interfaces.^{15–17} This is opposite to the case of most traditional III–V's, in which anion-rich growth is usually preferred. In 2007, King et al. reported an atomic scale study of the Ga autosurfactant effect

on the Ga-polar GaN surface using scanning tunneling microscopy (STM), giving new insight into the atomistic growth process.¹⁸ Clearly, Ga atoms are highly mobile at the Ga-rich GaN surface at room temperature, and more insights could be attained by investigating the surfaces at low temperatures and freezing out this motion.

In general, directly probing and individually manipulating single atoms (both magnetic and nonmagnetic) and molecules on surfaces is a topic of great interest and importance.^{19–25} In particular, the direct investigation of single adatoms on III–V semiconductor surfaces (for example arsenic, gallium, and manganese adatoms on GaAs(110)-1 × 1 surfaces, and indium adatoms on InAs(111)A-2 × 2 surfaces) have yielded unique insights into electronic and spintronic properties as well as atomic diffusion and surface growth.^{21,26,27}

In this Letter, we focus specifically on the behavior of native gallium adatoms on the atomically smooth nitrogen polar GaN surface, whose family of reconstructions [1 × 1, 3 × 3, 6 × 6, and c(6 × 12)] has been well known for many years.^{28,29} The study begins by carrying out MBE growth of N-polar GaN(000 $\bar{1}$) under slightly gallium-rich conditions (see

Received: December 28, 2014

Revised: February 3, 2015

Published: February 6, 2015

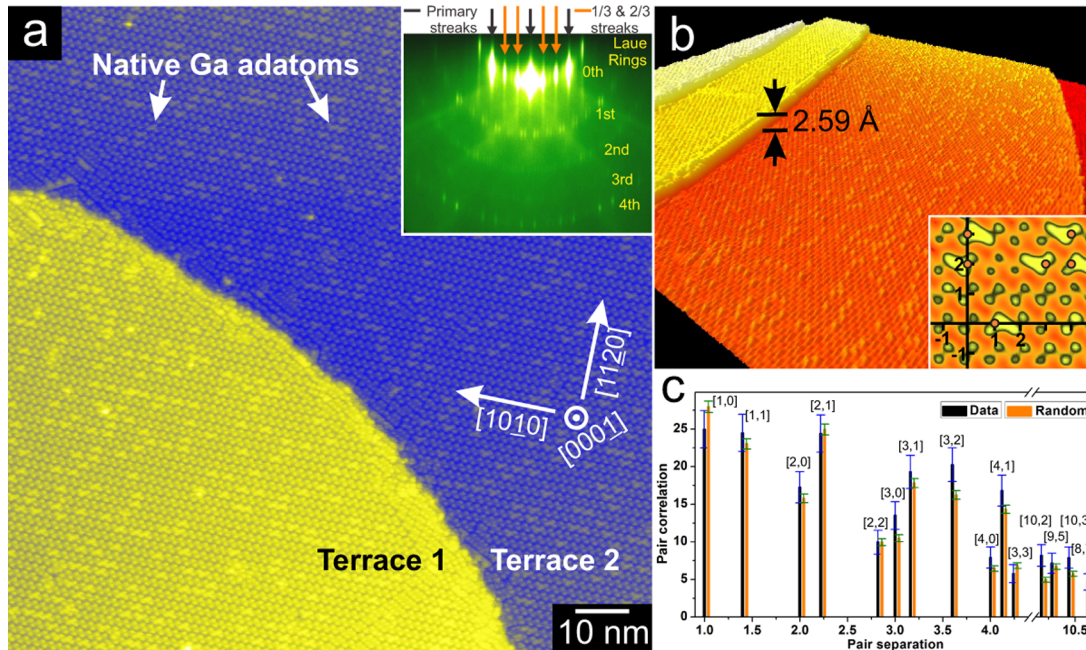


Figure 1. Randomly distributed point like defects on the $c(6 \times 12)$ reconstruction. (a) STM image of the as-grown N-polar GaN surface taken at LHe temperature showing atomically flat terraces having $c(6 \times 12)$ reconstruction rows and point like bright defects. Image size $130 \text{ nm} \times 130 \text{ nm}$, $V_s = 1.5 \text{ V}$; $I_t = 49 \text{ pA}$. Inset: characteristic $c(6 \times 12)$ RHEED pattern containing $3\times$ and $6\times$ streaks along with first five Laue rings. (b) 3D-rendered STM image obtained with $V_s = 1.5 \text{ V}$ and $I_t = 47 \text{ pA}$, where the bright defects extending along $c(6 \times 12)$ reconstruction rows can be seen clearly. Inset: Zoomed-in view where the defects appear in two distinct orientations L_U and L_D . An orthogonal $x-y$ grid is defined for calculating pair correlations. (c) Pair correlation of the L's on the GaN surface is plotted side by side with results obtained for a uniform discrete random distribution. Coordinate labels represent sets of pair separations, that is, $[1,0] = \{(1,0), (0,1)\}$.

Methods), resulting in the $c(6 \times 12)$ surface reconstruction after cooling the sample down to room-temperature (RT). The sample is then further cooled to $\sim 4.2 \text{ K}$ in a low-temperature STM (LT-STM) system. Examining the $c(6 \times 12)$ reconstructed surface at LT, we find new unexpected features never seen at RT, namely a high concentration (~ 3 trillion/ cm^2) of L-shaped Ga defects covering the surface. These features are located at asymmetrical adsorption sites within each of two chiral forms of the $c(6 \times 12)$. We show that these unusual-shaped features correspond to a two-dimensional gas of Ga atoms at the surface, related to equilibrium with Ga droplets, and which forms when the Ga coverage exceeds a certain limiting coverage (shown here to be $1/4 \text{ ML}$).

Presented in Figure 1a is a $130 \text{ nm} \times 130 \text{ nm}$ UHV LT-STM image of the N-polar $\text{GaN}(000\bar{1})$ surface having the $c(6 \times 12)$ reconstruction; two large atomic terraces are seen in the image separated by an atomic step of height 2.59 \AA . Uniaxial domains of the $c(6 \times 12)$ reconstruction cover the terraces as a row-like structure with rows running along $\langle 10\bar{1}0 \rangle$ at this positive sample bias of $+1.5 \text{ V}$. The $c(6 \times 12)$ reconstruction is widespread across the surface as indicated by the RHEED pattern shown in the inset of Figure 1a which was taken at the end of growth and after cooling the sample down to room temperature; the dominant streaks in the zeroth-order Laue ring have $3\times$ periodicity, while in addition $6\times$ streaks are faintly seen. While the first, second, third, and fourth-order Laue rings are all observed, the first and third-order rings are the most unique to the $c(6 \times 12)$, the first-order consisting of characteristic doublets of short streaks on a $3\times$ pattern.

What stands out clearly in the LT-STM image of Figure 1a are bright, point defect-like features which appear to be scattered randomly across the surface. These defects are located

at the centers of the $c(6 \times 12)$ rows; their concentration on this sample is $\sim 0.38\%$ of a monolayer (ML), one ML on $\text{GaN}(000\bar{1})$ corresponding to a density of $1.14 \times 10^{15} \text{ atoms/cm}^2$. Shown in Figure 1b is a 3-dimensional rendering of a similar surface where also the defect features can be seen extending along the row directions. As can be seen in the inset of Figure 1b, these defects appear with identical shapes resembling a boomerang or “L” shape and having two 180° -opposite rotational orientations within a given $c(6 \times 12)$ domain.

It should be emphasized that these point defect features have never been seen in UHV STM images taken at room temperature; so their identification is therefore of great interest. We can immediately rule out contaminants adsorbed from the vacuum chamber. Although the vacuum level during the experiment was $\sim 3 \times 10^{-10} \text{ Torr}$, more importantly the defect concentration was seen to be constant with scanning time; no change within the image was seen over a period of many hours (see Supporting Information). So, the features must be intrinsic to the sample (either N or Ga), and being that the growth was carried out under Ga-rich conditions, we can rule out N. To verify the features as Ga atoms, we carried out additional experiments (see Supporting Information) in which we varied the Ga flux during growth over a small range and observed a corresponding change in the defect concentration, proving that these L defects are Ga atoms.

What we can already therefore realize is that these frozen-out Ga atoms at LHe (liquid helium) temperature must be present and mobile at room temperature. They represent an excess of Ga from the growth which, combined with the Ga comprising the $c(6 \times 12)$ reconstruction itself, defines the Ga-rich growth conditions. So at room temperature in Ga-rich conditions, there

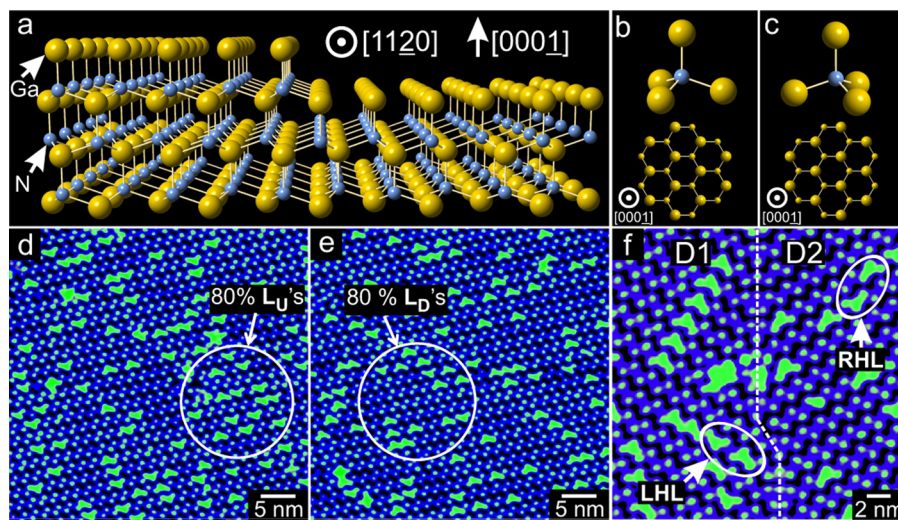


Figure 2. Two distinct orientations (L_U and L_D) and handedness [left-handed L (LHL) and right-handed L (RHL)] of the L and its relation to the GaN crystal structure. (a) GaN lattice is shown along $[11\bar{2}0]$, where it can be seen that the GaN crystal structure reverses upon crossing a bilayer height step (2.59 Å). (b, c) The 180° rotation can also be seen by looking at the lattice along $[0001]$. Images in (d) and (e) are zoom-ins taken from terraces 1 and 2 of Figure 1a, respectively. On terrace 1 (d), L_U 's are 4× more common than L_D 's, whereas on terrace 2 (e), L_D 's are 4× more common than L_U 's. These ratios are maintained even to small areas as encircled in the images. $V_s = 1.5$ V; $I_t = 49$ pA. (f) Two chiral enantiomeric domains of $c(6 \times 12)$ reconstruction on a single terrace. In domain 1 (D1) only LHL's can be seen, whereas in domain 2 (D2) only RHL's can be seen. LHL's and RHL's occur in both L_U and L_D orientations, as the pairs are encircled in the image. $V_s = 1.5$ V; $I_t = 32$ pA.

exists a two-dimensional gas of Ga atoms on the surface whose thermal energy exceeds the diffusion barrier across the $c(6 \times 12)$ reconstruction. Being frozen-out at LHe temperature, the diffusion barrier must lie within a small energy window (0.35–26 meV). These energies are much smaller than the 200 meV diffusion barrier for Ga adatoms on the Ga adlayer surface on GaN calculated by Zywiert et al.¹⁴

In order to determine if there is any preferential ordering between the frozen-out adatoms, pair correlation analysis was carried out on the Ga L's. Each Ga L's position was located as a coordinate pair on an orthogonal x - y grid (see inset of Figure 1b) having spacing of 1 unit of $c(6 \times 12)$ along $[10\bar{1}0]$ (x direction) and 1 unit of $c(6 \times 12)$ along $[11\bar{2}0]$ (y direction). An arbitrary region having 29 units along x and 25 units along y and containing ~100 coordinate pairs was entered into a pair correlation simulation program,³⁰ resulting in a pair correlation distribution; a second identically-sized region from a different terrace was again analyzed to get better statistics, and the resulting average is shown in Figure 1c in a bar graph. What is plotted is number of occurrences versus pair separation, with pairs always being separated by some combination of integer units along x and y . What we find is that almost every possible type of pair separation is found (e.g., $[1,0]$, $[1,1]$, $[2,0]$, $[2,1]$) with finite probability.

The resulting pair correlation from the GaN data is compared to the pair correlation resulting from a uniform discrete random distribution of points having the same spatial density. The random pair correlation simulation was carried out seven times and then an average was taken, and this is also presented in Figure 1c. Looking over the results, it is seen for the GaN data and the random data that there is a similar characteristic dependence on pair separation with, for example, the $[2,0]$ correlation being ~33% less probable than the $[2,1]$ correlation which is itself however ~140% more probable than the $[2,2]$ correlation. The main point, however, is that the GaN pair correlations agree very well with the correlations from the uniform discrete random distribution, usually to within 1σ .

What we can therefore conclude is that the Ga L's are distributed randomly, the definition of a gas.

In order to understand how the Ga atom gas condenses onto the cold GaN surface, it is important to realize that although the $c(6 \times 12)$ reconstruction looks exactly the same on either side of the step seen in Figure 1a, the underlying GaN lattice is rotated 180°. To see this, shown in Figure 2a is a 3-dimensional perspective-view rendering of the GaN lattice, as seen from the side (along $[11\bar{2}0]$), illustrating a single unit-height GaN step (one bilayer, corresponding to the 2.59 Å steps seen in the STM images in Figure 1). Clearly, the bonding at the surface is dependent upon the 3-fold symmetry of the wurtzite GaN crystal structure, and the orientation of the bonds can be seen to rotate by 180° across the step. For example, just consider how the surface N atoms' bonds rotate across the step, expanded in Figure 2b and c. This local bonding asymmetry across a unit-height step at the surface has a very big effect on the sites for Ga atom condensation.

As noted already from Figure 1, the Ga defects appear in two different rotational orientations. As presented in Figure 2d, it can be easily seen that these two orientations do not occur in equal fractions; in fact, it is found that ~80% have one orientation (L_U , $U \equiv$ “up”) and the other ~20% have the opposite orientation (L_D , $D \equiv$ “down”). The existence of a 4:1 probability ratio for $L_U:L_D$ suggests the existence of two or more inequivalent binding sites for the frozen-out Ga adatoms within each $c(6 \times 12)$ unit cell.

It is furthermore found that these inequivalent fractions interchange upon crossing a single unit-height bilayer step on the surface, as illustrated in Figure 2e in which there are found ~80% L_D 's and ~20% L_U 's. Clearly then, the asymmetry in the L-orientation fractions across the unit-height step is directly related to the bond rotation shown in Figure 2b,c. This further proves the existence of two or more inequivalent bonding sites for the Ga atoms within a $c(6 \times 12)$ unit cell. And in addition, it suggests looking carefully at the model for the $c(6 \times 12)$ in order to identify the location of the asymmetric bonding sites.

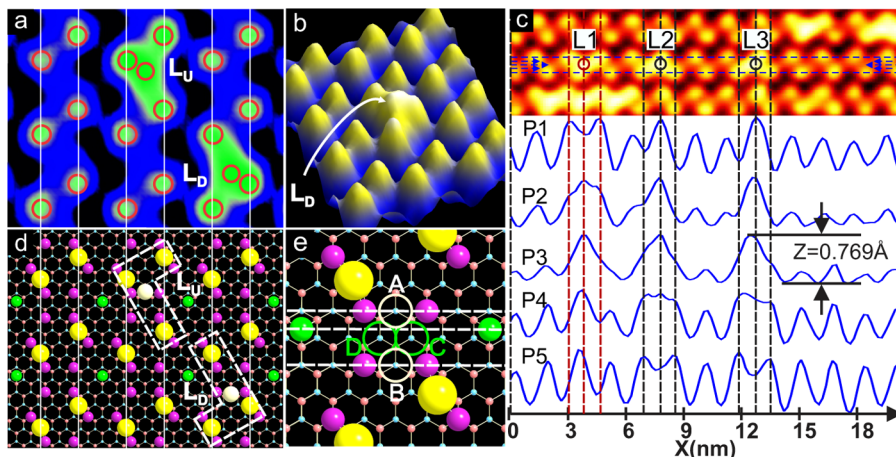


Figure 3. L_U and L_D formations and the probable sticking sites of excess Ga atoms. (a) L_U and L_D orientations of the RHL are shown in the STM image taken with $V_s = 1.5$ V; $I_t = 32$ pA. Red-colored circles correspond to yellow and white-colored balls in the model shown in (d). (b) 3D-rendered STM image showing the atomic structure of an L. A peak at the center of the L can be seen clearly. $V_s = 2.5$ V; $I_t = 26$ pA. (c) Series of 5 line profiles (P1–P5) are taken across one L_U (L1) and two L_D 's (L2 and L3). P1 shows a double peak for L1 and single peaks for L2 and L3, whereas P5 shows a single peak for L1 and double peaks for L2 and L3. Small bumps approximately at the center of the double peaks of L1 and L2 are visible in P2 and P4, respectively. P3 shows single peaks near the centers of the 3 L's. $V_s = 1.5$ V; $I_t = 49$ pA. (d) Detailed model of the $c(6 \times 12)$ reconstruction with L_U and L_D schematics is shown. The white colored balls occupying bridge sites are responsible for the formation of the L's. (e) Zoomed-in view of the model where it can be seen that site A and site B are identical with respect to yellow and pink colored balls but are asymmetrical with respect to peach and green-colored balls.

Before proceeding to identify the preferred surface bonding sites for the Ga defects, one final observation can be made, which concerns the inherent chirality of an “L” shape. Considering Figure 2d,e, only left-handed L's are seen, in both orientations and in unequal fractions within a given terrace. Nonetheless, both right-handed as well as left-handed L's are found on the sample surface, as depicted within a single surface region shown in Figure 2f. Right-handed L's only require the formation of a right-handed $c(6 \times 12)$ domain, as even the reconstruction itself is seen to be chiral. A given chirality is selected as the $c(6 \times 12)$ forms during cooling. As seen in Figure 2f, the two chiral domains are mirror-symmetric with respect to each other, and it is found that the 4:1 ratio of orientation probabilities occurs for both chiralities.

Shown in Figure 3a is a zoom-in view LT-STM image of a region of $c(6 \times 12)$ containing two right-handed Ga defects (L's) in each of the two opposite orientations: labeled L_U and L_D . Three zig-zagging rows along the vertical direction, each containing three pairs of Ga adatoms (red-circled bright spots) constitute the basic appearance of the $c(6 \times 12)$ reconstruction itself within the image. In Figure 3d is shown a detailed model for the $c(6 \times 12)$ reconstruction matching the STM region in Figure 3a exactly (see Supporting Information, Figure S3, regarding the model). Each Ga adatom in the STM image corresponds to a Ga atom bridge site in the model.²⁹ The three atoms forming a bridge consist of one Ga adatom (yellow balls in the model) bonded to two other Ga atoms (pink balls in the model) which are bonded to the underlying GaN bilayer via a Ga-termination (peach-colored balls, referred to as the Ga adlayer).²⁸ The adlayer Ga atoms are back-bonded directly underneath to the N atoms of the bilayer (refer to Figure 2b,c). Additional adatom features are also identified in STM images (green balls, see Supporting Information). In total we find for the $c(6 \times 12)$, that the Ga adatom density is 1/4 ML, corresponding to the limiting Ga coverage on N-polar GaN(000̄1).

Detailed image analysis is used to address several key questions, including the nature of the frozen-out Ga defect, the origin of the two “L” orientations (L_U and L_D), and why one “L” orientation is strongly favored over the other (4:1 ratio). It is clearly seen from the STM image of Figure 3a that the “L” shapes are a natural consequence of the $c(6 \times 12)$ reconstruction. The presence of a Ga adatom defect enhances the empty states in a localized region surrounding itself, including the three neighboring Ga adatoms within the zigzag row, for example within the dash-boxed regions shown in Figure 3d. The two “L” orientations thus arise based on exactly which three adatoms are involved, which in turn depends on the exact site location of the frozen-out Ga. Interestingly, this local enhancement at positive biases is not found at negative biases (see Supporting Information).

To get an idea of the site location of the frozen-out Ga, a 3-dimensional perspective view of one of the right-handed L's is presented in Figure 3b, which reveals a strong central peak nestled between 3 Ga adatom peaks corresponding to the “L”. The Ga atom defect is centered approximately halfway between the two ends of the “L” along the row and approximately halfway between the rows of adatoms on either side across the row. To make a more careful measurement, line profile analysis is performed, as shown in Figure 3c. Here, five horizontal line profiles (P1–P5) are taken across three L's (labeled L1, L2, and L3) located within the middle $c(6 \times 12)$ row of the presented STM image. Profile P1 (at top) shows a double-peak structure across the two ends of L1 and single peaks across the corners of L2 and L3. Profile P5 (at bottom) shows similar double peak structures across the two ends of L2 and L3 and a single peak across the corner of L1. Profiles P2 and P4 reveal small bumps popping up midway between the double peaks. And finally, profile P3 reveals exactly the peak position of the Ga atom defect, and its height is measured as 0.77 Å, which is similar to or slightly above the height of the Ga adatoms (refer to Figure 3b). So then, the Ga adsorption sites are near the geometrical centers of the L's.

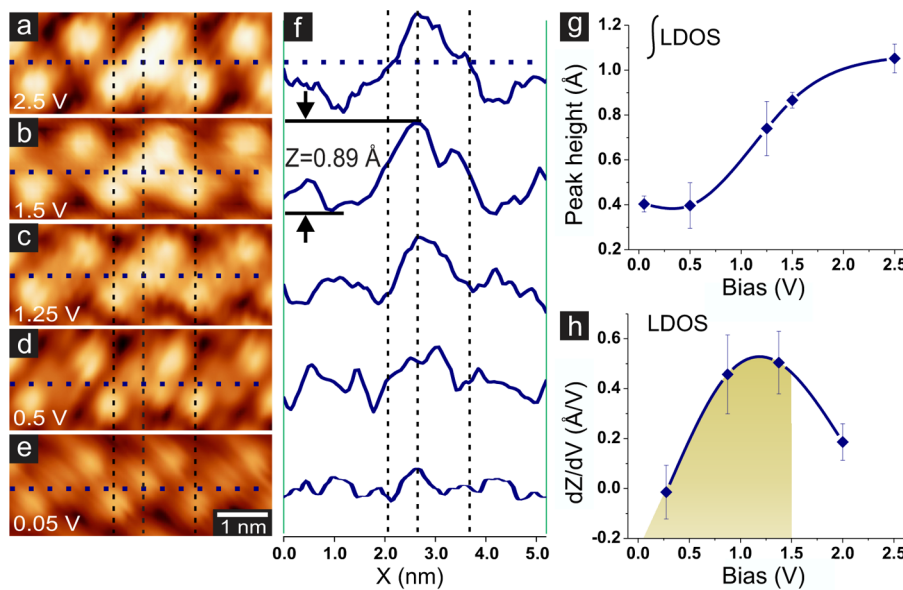


Figure 4. Bias dependence and LUMO level of the L's. (a–e) STM images as a function of bias showing how intensity of the L varies. Intensity gradually increases with increase in bias voltage and saturates around 1.5 V; corresponding line profiles across the L's are presented in (f). Scanning parameters are (a) $V_s = 2.5$ V, $I_t = 26$ pA; (b) $V_s = 1.5$ V, $I_t = 32$ pA; (c) $V_s = 1.25$ V, $I_t = 28$ pA; (d) $V_s = 0.5$ V, $I_t = 24$ pA; (e) $V_s = 0.05$ V, $I_t = 24$ pA. (g) Peak height (L intensity) is plotted versus bias voltage. The curve has an S shape saturating at higher biases. (h) Numerical derivative of the peak height versus bias, corresponding to the local density of states, peaking around 1.2 V.

This information helps to identify possible site locations of the adsorbed Ga adatoms, as indicated in the close-up model shown in Figure 3e; here, one identifies two possible bridge site positions, as indicated by the white circles labeled A and B. These two bridge sites are at the geometrical centers of the two possible L's, one being an L_U , one being an L_D . The A and B sites have the same bridge site geometry as for the regular Ga adatoms (yellow balls) of the $c(6 \times 12)$, namely they are T4 bridge sites. And furthermore, the A and B sites are the only remaining T4 bridge sites at the surface not already occupied by Ga atoms. So certainly sites A and B are likely binding sites.

What cannot easily be answered is why one L orientation is favored over the other by a 4:1 ratio. If the two adsorption sites were identical, the probabilities should be equal. However, it is seen from Figure 3e that the two T4 bridge sites are not identical; so this could lead to the asymmetrical adsorption. For example, relative to the nearby Ga adatoms (yellow balls), the Ga adlayer bonding angles are 180° reversed at the location of the A and B sites. The reversal in the probabilities for L_U and L_D from 4:1 to 1:4 across a single bilayer-height step could therefore be related to the 180° reversal of the underlying GaN lattice.

To gain further insights into the origins of the bonding probabilities, it is important to consider the energy dependence of the L defects (Note: the full bias-dependence of the $c(6 \times 12)$ reconstruction was previously shown by Smith et al.²⁹). Presented in Figure 4a–e are zoomed-in STM images of an L defect over a range of different voltage biases beginning from +2.5 V (a) and reducing to +1.5 V (b), +1.25 V (c), +0.5 V (d), and +0.05 V (e) (for negative bias, see Supporting Information). It is first of all noticed that the L defect shows up much more strongly at higher bias voltages away from the Fermi energy (E_F) and can barely be seen near E_F . This is also seen clearly in Figure 4f which shows corresponding line profiles taken across the center of the L defect as a function of bias voltage.

It is noticed from this set of line profiles that the adatom peak is located off-center relative to the two ends of the L at all shown biases (except it is difficult to tell at +0.5 V); corresponding to this, two additional adsorption site possibilities (also bridge sites) are identified in Figure 3e as site C (for L_U) and site D (for L_D). It is possible that multiple (4, 5, or more) different binding sites actually occur (with various probabilities), leading to subtle variations in the L's shapes which we can see by careful inspection of images shown in Figure 2.

Looking at the energy dependence, we plot the peak height of the L defect as a function of bias voltage in Figure 4g, where the trend (shown as the solid line) of increasing height with bias is clearly shown; in addition, the peak height appears to saturate near 2.0–2.5 V. Given that the peak (tip) height corresponds to an integral of the local density of states of the surface, the derivative is therefore proportional to the local density of states of the surface. This is plotted in Figure 4h, where a peak is seen as a function of bias voltage, with the centroid of the peak located near ~ 1.2 V. This peak can be interpreted as a LUMO (lowest unoccupied molecular orbital) or antibonding state for the Ga adatom and the $c(6 \times 12)$ surface. Thus, we can estimate ~ 2.4 eV (2× the LUMO energy) as the binding energy for Ga atoms to the $c(6 \times 12)$ surface (much greater than the diffusion barrier), which explains why they stay on the surface at temperatures up to ~ 700 °C. This estimate is in relatively good agreement with the finding of 2.8 eV for the activation energy for Ga atoms desorbing from the GaN surface within the Ga-rich regime by Heying et al.³¹

Clearly, the direct observation of a frozen-out gas of native Ga adatoms at the N-polar GaN(0001) surface solidifies the understanding of gallium rich growth, considered key to the success of nitride MBE growth technology. How this native Ga gas furthermore would react to foreign adsorbates such as other group III atoms (Al, In) or to transition metal atoms (Mn, Fe,

etc.) will be of great interest for advancing electronic and spintronic materials development within the nitrides. Looking beyond nitrides, it would be interesting to explore whether similar phenomena occur in other semiconductor systems, and if so, this could also lead to new understandings of surface growth kinetics in those systems.

Methods. The experiments are performed in a custom designed ultrahigh vacuum (UHV) system combining MBE with LT-STM which allows to study the as-grown sample without exposure to air.³² The N-polar GaN(0001) thin film is grown on a sapphire(0001) substrate initially cleaned ex situ with acetone followed by isopropyl-alcohol and further cleaned in situ by heating the substrate to 1000 °C while being exposed to a nitrogen plasma flux for ~30 min. MBE growth is carried out using a Ga effusion cell providing a flux of $\sim 3 \times 10^{14}$ Ga atoms/(cm² s) (see Supporting Information) in combination with a N flux coming from an RF N Plasma Source (SVTA) operated at a forward power setting of 450 W and using N₂ as the source gas. The sample temperature during growth is estimated to be 730 ± 30 °C. During growth, the sample surface is monitored using RHEED which gives characteristic patterns corresponding to different surface reconstructions. The growth is terminated by simultaneously closing the Ga shutter and switching off the RF plasma source power, after which the sample temperature is slowly ramped down to room temperature. After completion of the growth by MBE, the fresh sample is transferred in situ from the growth chamber into a central distribution chamber and then into the LT-STM chamber. The sample is maintained under high or ultrahigh vacuum during all the transfer process. The base pressure of the LT-STM chamber was $\sim 3.0 \times 10^{-10}$ Torr. Once inside the LT-STM, the sample (as well as the tip) cool down using LHe to base temperature (close to 4.2 K) before initiating scanning. STM images are acquired using constant current mode; and STM data is collected, for a given surface, over periods of up to 3 days.

■ ASSOCIATED CONTENT

Supporting Information

Constancy of the L feature density with time; L feature concentration versus Ga flux during growth; and positive/negative bias STM images of c(6 × 12) reconstruction with one L feature. This material is available free of charge via the Internet at <http://pubs.acs.org/>.

■ AUTHOR INFORMATION

Corresponding Author

*E-mail: ohiousmith@gmail.com. Fax: +1-740-593-0433.

Notes

The authors declare no competing financial interest.

■ ACKNOWLEDGMENTS

Research has been supported by the U.S. National Science Foundation, Division of Materials Research, under Award # DMR-1206636 (K.A.) and by the U.S. Department of Energy, Office of Basic Energy Sciences, Division of Materials Sciences and Engineering under Award # DE-FG02-06ER46317 (A.F.). The authors would also like to acknowledge the WSxM software for image processing.³³

■ REFERENCES

- (1) Nakamura, S.; Senoh, M.; Mukai, T. *Appl. Phys. Lett.* **1993**, *62*, 2390–2392.
- (2) Nakamura, S.; Mukai, T.; Senoh, M. *Appl. Phys. Lett.* **1994**, *64*, 1687–1689.
- (3) Nakamura, S. nobelprize.org. Nobel Media AB 2014. Web. http://www.nobelprize.org/nobel_prizes/physics/laureates/2014/nakamura-facts.html (accessed Dec 18 2014).
- (4) Morkoc, H.; Strite, S.; Gao, G.; Lin, M.; Sverdlov, B.; Burns, M. J. *Appl. Phys.* **1994**, *76*, 1363–1398.
- (5) Pengelly, R. S.; Wood, S. M.; Milligan, J. W.; Sheppard, S. T.; Pribble, W. L. *IEEE Trans. Microwave Theory Tech.* **2012**, *60*, 1764–1783.
- (6) Jewett, S. A.; Makowski, M. S.; Andrews, B.; Manfra, M. J.; Ivanisevic, A. *Acta Biomater.* **2012**, *8*, 728–733.
- (7) Kim, H.; Colavita, P. E.; Metz, K. M.; Nichols, B. M.; Sun, B.; Uhrlrich, J.; Wang, X.; Kuech, T. F.; Hamers, R. J. *Langmuir* **2006**, *22*, 8121–8126.
- (8) Ito, T.; Forman, S. M.; Cao, C.; Li, F.; Eddy, C. R., Jr.; Mastro, M. A.; Holm, R. T.; Henry, R. L.; Hohn, K. L.; Edgar, J. *Langmuir* **2008**, *24*, 6630–6635.
- (9) Qian, W.; Rohrer, G.; Skowronski, M.; Doverspike, K.; Rowland, L.; Gaskill, D. *Appl. Phys. Lett.* **1995**, *67*, 2284–2286.
- (10) Xie, M.; Seutter, S.; Zhu, W.; Zheng, L.; Wu, H.; Tong, S. *Phys. Rev. Lett.* **1999**, *82*, 2749.
- (11) Lee, S. M.; Lee, Y. H.; Hwang, Y. G.; Elsner, J.; Porezag, D.; Frauenheim, T. *Phys. Rev. B* **1999**, *60*, 7788.
- (12) Kim, H.-Y.; Booth, E. C.; Mbaye, M. T.; Gatica, S. M. *J. Low Temp. Phys.* **2014**, *175*, 590–603.
- (13) Mitchell, C. C.; Coltrin, M. E.; Han, J. *J. Cryst. Growth* **2001**, *222*, 144–153.
- (14) Zywietsz, T.; Neugebauer, J.; Scheffler, M. *Appl. Phys. Lett.* **1998**, *73*, 487–489.
- (15) Lee, C.; Sagar, A.; Feenstra, R. M.; Inoki, C.; Kuan, T.; Sarney, W.; Salamanca-Riba, L. *Appl. Phys. Lett.* **2001**, *79*, 3428–3430.
- (16) Monroy, E.; Sarigiannidou, E.; Fossard, F.; Gogneau, N.; Bellet-Amalric, E.; Rouviere, J.-L.; Monnoye, S.; Mank, H.; Daudin, B. *Appl. Phys. Lett.* **2004**, *84*, 3684–3686.
- (17) Gogneau, N.; Sarigiannidou, E.; Monroy, E.; Monnoye, S.; Mank, H.; Daudin, B. *Appl. Phys. Lett.* **2004**, *85*, 1421–1423.
- (18) King, S.; Weinert, M.; Li, L. *Phys. Rev. Lett.* **2007**, *98*, 206106.
- (19) Stroscio, J. A.; Eigler, D. *Science* **1991**, *254*, 1319–1326.
- (20) Yayon, Y.; Brar, V.; Senapati, L.; Erwin, S.; Crommie, M. *Phys. Rev. Lett.* **2007**, *99*, 067202.
- (21) Kitchen, D.; Richardella, A.; Tang, J.-M.; Flatté, M. E.; Yazdani, A. *Nature* **2006**, *442*, 436–439.
- (22) Meyer, G.; Moresco, F.; Hla, S. W.; Repp, J.; Braun, K.-F.; Fölsch, S.; Rieder, K. H. *Jpn. J. Appl. Phys.* **2001**, *40*, 4409.
- (23) Hla, S.-W.; Braun, K.-F.; Iancu, V.; Deshpande, A. *Nano Lett.* **2004**, *4*, 1997–2001.
- (24) Rao, B. V.; Kwon, K. Y.; Liu, A. W.; Barlets, L. *Proc. Natl. Acad. Sci. U.S.A.* **2004**, *101*, 17920–17923.
- (25) Limot, L.; Pehlke, E.; Kröger, J.; Berndt, R. *Phys. Rev. Lett.* **2005**, *94*, 036805.
- (26) Gwo, S.; Smith, A.; Shih, C. *J. Vac. Sci. Technol. A* **1993**, *11*, 1644–1648.
- (27) Yang, J.; Nacci, C.; Martínez-Blanco, J.; Kanisawa, K.; Fölsch, S. *J. Phys. Cond. Mater.* **2012**, *24*, 354008.
- (28) Smith, A.; Feenstra, R.; Greve, D.; Neugebauer, J.; Northrup, J. *Phys. Rev. Lett.* **1997**, *79*, 3934.
- (29) Smith, A.; Feenstra, R.; Greve, D.; Neugebauer, J.; Northrup, J. *Appl. Phys. A: Mater. Sci. Process.* **1998**, *66*, S947–S951.
- (30) Valmianski, I. *Matlab application: Two point correlation function of a finite 2D lattice*; MATLAB Central/Mathworks: Natick, MA, 2011.
- (31) Heying, B.; Averbeck, R.; Chen, L.; Haus, E.; Riechert, H.; Speck, J. *J. Appl. Phys.* **2000**, *88*, 1855–1860.
- (32) Lin, W.; Foley, A.; Alam, K.; Wang, K.; Liu, Y.; Chen, T.; Pak, J.; Smith, A. R. *Rev. Sci. Instrum.* **2014**, *85*, 043702.

(33) Horcas, I.; Fernández, R.; Gomez-Rodriguez, J.; Colchero, J.; Gómez-Herrero, J.; Baro, A. *Rev. Sci. Instrum.* **2007**, *78*, 013705.